

The impact of the halide cage on the electronic properties of fully inorganic caesium lead halide perovskites

Z. Yang,[†] A. Surrente,[†] K. Galkowski,^{†,‡} A. Miyata,[†] O. Portugall,[†] R. J. Sutton,[¶] A. A. Haghighirad,[¶] H. J. Snaith,[¶] D. K. Maude,[†] P. Plochocka,^{*,†} and R. J. Nicholas^{*,¶}

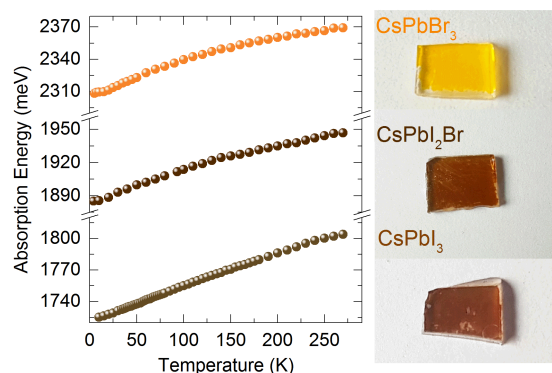
[†]*Laboratoire National des Champs Magnétiques Intenses, CNRS-UGA-UPS-INSA, 143, avenue de Rangueil, 31400 Toulouse, France*

[‡]*Institute of Experimental Physics, Faculty of Physics, University of Warsaw - Pasteura 5, 02-093 Warsaw, Poland*

[¶]*University of Oxford, Clarendon Laboratory, Parks Road, Oxford, OX1 3PU, United Kingdom*

E-mail: paulina.plochocka@lncmi.cnrs.fr; robin.nicholas@physics.ox.ac.uk

Graphical TOC Entry



Abstract

Perovskite solar cells with record power conversion efficiency are fabricated by alloying both hybrid and fully inorganic compounds. While the basic electronic properties of the hybrid perovskites are now well understood, key electronic parameters for solar cell performance, such as the exciton binding energy of fully inorganic perovskites, are still unknown. By performing magneto transmission measurements, we determine with high accuracy the exciton binding energy and reduced mass of fully inorganic CsPbX₃ perovskites (X=I, Br, and an alloy of these). The well behaved (continuous) evolution of the band gap with temperature in the range 4 – 270 K suggests that fully inorganic perovskites do not undergo structural phase transitions like their hybrid counterparts. The experimentally determined dielectric constants indicate that at low temperature, when the motion of the organic cation is frozen, the dielectric screening mechanism is essentially the same both for hybrid and inorganic perovskites, and is dominated by the relative motion of atoms within the lead-halide cage.

Rapid developments in the field of hybrid organic-inorganic perovskites have led to a dramatic increase of power conversion efficiencies in perovskite-based solar cells, which currently exceed 22%.¹⁻⁴ Hybrid organic-inorganic perovskites combine low-cost fabrication processes^{5,6} with strong light absorption,⁷ efficient photoluminescence,^{8,9} together with long carrier lifetimes and diffusion lengths.^{10,11} The combination of these properties has led to numerous applications of this class of materials in optoelectronic devices beyond solar cells, including light emitting diodes,¹² lasers¹³ and photodetectors.¹⁴

Hybrid organic-inorganic perovskites are characterized by a general chemical formula ABX_3 , where A is an organic ammonium cation (Methylammonium (MA), or formamidium, FA), $B=Pb^{2+}$ or Sn^{2+} and X is a halide anion (Cl^- , Br^- , I^- or an alloyed combination of these). Initially, the fabrication of perovskite-based solar cells was based on mono halide material.¹⁵ In this case, the power conversion efficiency is usually limited to less than 20% for conventional $MAPbI_3$ based devices,¹⁶ which are additionally plagued by poor resistance to moisture or high temperatures,^{17,18} as well as by the formation of trap states induced by exposure to light.¹⁹ The synthesis of $FAPbI_3$ provides, in principle, an attractive alternative, as it has a band gap smaller than its MA counterpart,²⁰ being closer to the optimal value for a single junction solar cell, which influences favorably its conversion efficiency.^{1,21} However, the large radius of the FA cation favors the formation of a photoinactive polymorph at room temperature.²² Alternatively, fully inorganic Caesium-based $CsPbX_3$ perovskite compounds²³ with an excellent thermal stability up to 450 °C^{24,25} have been explored as light harvesters.²⁶⁻²⁸ Their use is partially hindered by the large band gap in the case of $CsPbBr_3$ ²⁷ and by the high temperature formation of the photoactive polymorph, stable in ambient conditions for the lower band gap $CsPbI_3$.²³

The advantages of hybrid and inorganic perovskite families can be combined by introducing some amount of lighter inorganic cations into the organic lattice. Small molar fractions of Cs act as a crystallizer for the photoactive $FAPbI_3$ phase,^{29,30} also reducing halide phase segregation.³¹ The improvement of structural properties, resulting in superior morphology,^{2,31}

is accompanied by record solar cell efficiencies and by significantly improved stability under standard operation conditions.^{2,3} Alloyed Cs- and FAPbI₃ (band gap ~ 1.73 eV) has been employed in perovskite-silicon tandem solar cells,^{28,30,31} while the lower band gap FA/MA mixtures containing very small molar fractions of Caesium and Rubidium have demonstrated record high efficiencies exceeding 22% in a single-junction architecture.^{2,3} Despite the impressive performance of mixed cation devices, very little is known about the fundamental electronic properties of these materials. Moreover, a detailed knowledge of the electronic structure of fully inorganic perovskites is a crucial element for understanding the impact of the inorganic cation on the electronic properties of mixed compounds. Quantities relevant for photovoltaic applications, such as the exciton binding energy, the presence of the phase transition and dielectric screening have not as yet been experimentally investigated in CsPbX₃.

In this work, we present the results of systematic studies of the electronic and optical properties of inorganic CsPbX₃ layers, where X = Br, I or an alloy of the two, which have been heat treated to be in the metastable cubic black perovskite phase. Temperature dependent absorption measurements demonstrate no evidence for any phase transitions below 300 K in a striking contrast to their organic counterparts. We determine the exciton binding energy (R^*) and reduced mass (μ) by magneto transmission spectroscopy. Similarly to previous results obtained for hybrid organic inorganic compounds, we find that both exciton binding energy and reduced mass scale linearly with the band gap energy.^{32,33} The small binding energy of the exciton in CsPbI₃ compared to the thermal energy at room temperature suggests that in typical operational conditions for solar cells, photo-created species exhibit a free-carrier-like behavior, which makes CsPbI₃ an excellent building block for stable, high efficiency devices.^{2,3} Based on the value of binding energy, we have calculated the dielectric constant (ϵ_{eff}) and compared it with the values for organic inorganic counterparts. Interestingly, ϵ_{eff} is comparable for all the iodide compounds, but decreases significantly for the bromides. This suggests that at low temperature, when the motion of the organic cations

is frozen,³⁴ the dielectric screening mechanism is essentially the same for both the inorganic and hybrid perovskites and is controlled by the lead-halide cage.

Typical transmission spectra of CsPbBr₃, CsPbI₂Br and CsPbI₃, measured over a wide range of temperatures (4.2 K - 270 K), are presented in Fig. 1(a-c). We observe a consistent blue shift of the band edge absorption energy of CsPbI₃ through mixed CsPbI₂Br to CsPbBr₃, highlighting the good tuneability of the band gap via the introduction of a heavier halide in the crystal.³⁵ The transmission spectrum for each compound exhibits a single minimum at all temperatures, which blue shifts and broadens with increasing temperature. The detailed evolution of the band gap absorption energy with temperature is presented in Fig. 1(d). We note that the band gaps of all the investigated samples exhibit a well behaved monotonic dependence on the temperature. This is in stark contrast with organic-inorganic halide perovskites, where an increase in the band gap is observed at temperatures corresponding to the phase transitions to a lower symmetry crystalline structure.^{32,33,36-39} This is a particularly significant result in the case of CsPbI₃, which suggests that our sample preparation procedure (see Experimental Methods) preserves the photoactive perovskite phase of this compound even at cryogenic temperatures. Importantly, we have monitored the absorption spectra of all the samples during the cool down. This point was critical especially for the CsPbI₃, which is known to be unstable at ambient conditions. In the absorption spectra we did not see any signs of dramatic change of the band gap, which would suggest the transition into yellow phase. This supports our finding that we freeze the sample in the cubic phase. In the case of CsPbBr₃, we have investigated both as prepared samples (orthorhombic phase) and samples, which have been annealed at 250 °C, which is above the transition to the cubic phase.^{27,40} The identical transmission data and evolution of the gap with temperature shown in Fig. 1(a,d) demonstrate that annealing does not influence the electronic structure of CsPbBr₃ under the measurements conditions used. This suggests that independently of the thermal processing, CsPbBr₃ will always transform to the orthorhombic phase below the phase transition point at 88 °C and the continuous evolution of its band gap with temperature indicates the absence

of any further phase transitions and to a good stability of the investigated samples.

Low temperature magneto transmission spectroscopy is a powerful technique which has previously been used to precisely determine the binding energy and reduced mass of the exciton in organic-inorganic perovskites.^{32,33,39} In Fig. 2(a) we present typical magneto transmission spectra of CsPbBr₃ measured at 2 K. Related magneto transmission spectra of CsPbI₃ and CsPbI₂Br are shown in the Supporting Information (Fig1 SI). The pronounced minimum at ~ 2313 meV is attributed to the 1s excitonic state. With increasing magnetic field, we observe a clear blue shift of this transition. On the high energy side of the 1s transition, a weak minimum can be resolved for magnetic fields larger than 35 T. It is more clearly seen in differential transmission spectra obtained by dividing the transmission spectra by the spectrum measured at zero magnetic field (see Fig. 2(b)). At higher energy range, there are some hints of absorption due to free carrier transitions between Landau levels in the valence and conduction bands. To better resolve the free carrier transitions, we have extended the long pulse measurements to higher magnetic fields ($B > 70$ T) using the short pulse generated by a single turn coil (see Experimental Methods) to follow the absorption minima to higher energies. Representative magneto transmission curves measured with a single turn coil are presented in Fig. 2(c). These curves show the evolution of the transmission through the sample of a monochromatic (laser) light of different wavelengths measured as a function of the magnetic field. The minima correspond to dipole allowed transitions between Landau levels in the conduction and valence band.

To model the data further we plot the energetic positions of the minima observed in the absorption spectra as a function of the magnetic field, as marked by blue and black points in Fig. 3. The analysis of the full magnetic field dependence of both hydrogenic and free carrier transitions, shown in Fig. 3, enables us to extract the exciton binding energy and reduced mass.^{32,33,39} We introduce a dimensionless parameter $\gamma = \hbar\omega_c/2R^*$, where $\omega_c = eB/\mu$ is the cyclotron frequency of charge carriers and $\mu^{-1} = m_e^{-1} + m_h^{-1}$ defines the exciton reduced mass. In the high magnetic field limit (corresponding to $\gamma > 1$), the observed absorption

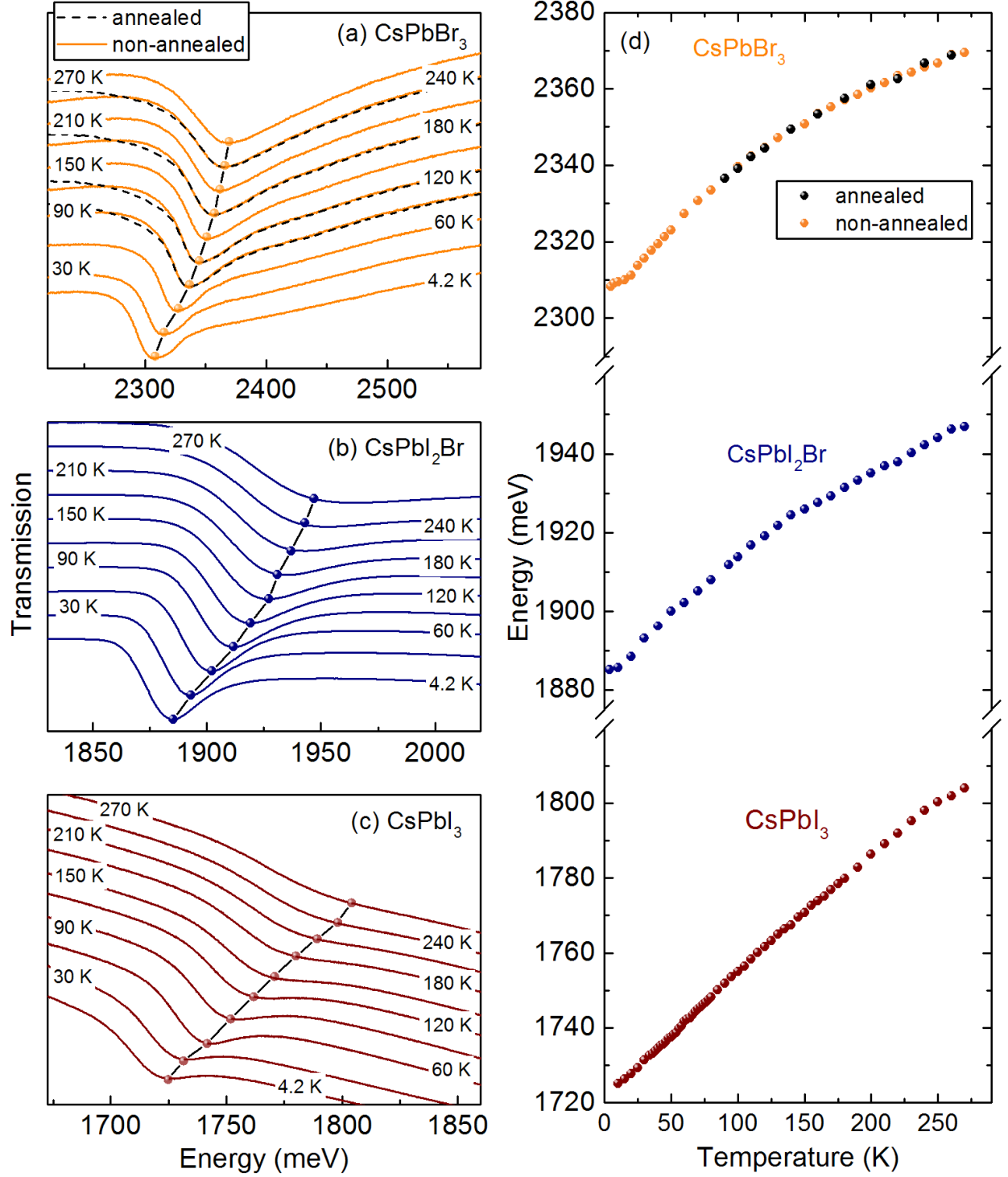


Figure 1: Transmission spectra measured at different temperatures for (a) CsPbBr₃, (b) CsPbI₂Br and (c) CsPbI₃. Symbols highlight the evolution of the 1s absorption with temperature. (d) Energy of the 1s transition (reflecting the evolution of the band gap) as a function of temperature for the three compounds. For CsPbBr₃ data is shown for the as prepared and annealed samples as described in the text.

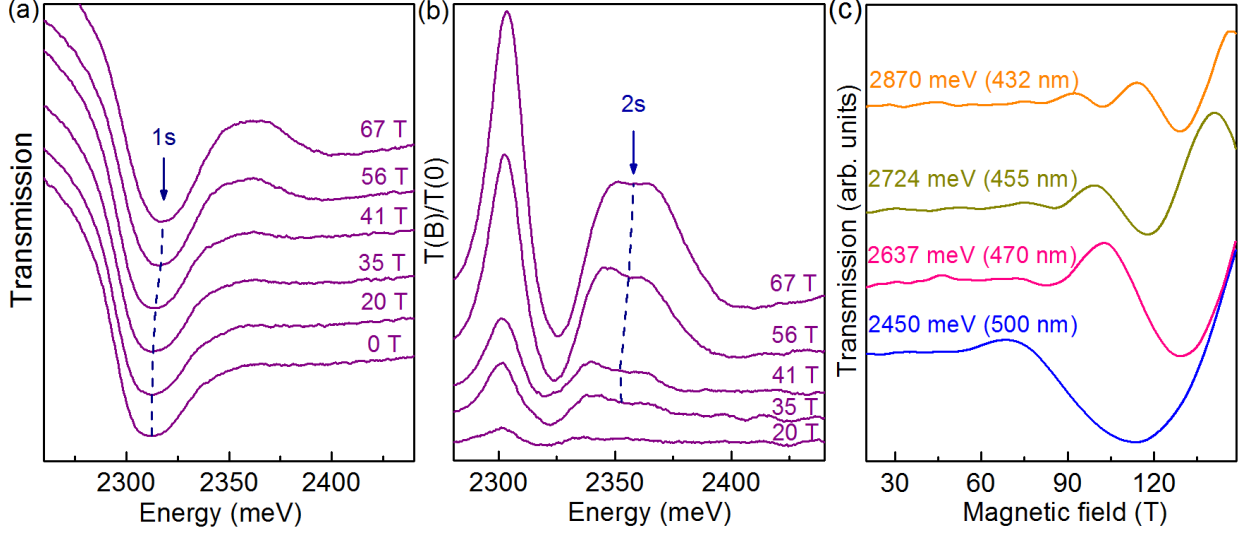


Figure 2: Low temperature transmission spectra in magnetic field for CsPbBr₃. (a) Transmission spectra measured at the indicated magnetic field values. (b) Transmission spectra in magnetic field divided by zero field spectrum. (c) Monochromatic transmission as a function of magnetic field obtained by the short pulse technique.

resonances are related to free carrier inter Landau level transitions with energies

$$E = E_g + \left(n + \frac{1}{2}\right) \hbar\omega_c, \quad (1)$$

where E_g is the band gap, $n = 0, 1, 2, \dots$ is the orbital quantum number of the Landau levels in the conduction and valence bands. For dipole allowed transitions ($\Delta n = 0$), and for a well-defined value of the band gap E_g , the only fitting parameter in Eq.(1) is the reduced mass μ . Fitting the observed resonances to Eq.(1) (gray lines in Fig.3) allows us to determine the exciton reduced mass. The excitonic like transitions close to the band edge are well described with a numerical model for a hydrogen atom in high magnetic field.⁴¹ The eigenenergies of an excitonic system in zero field are given by

$$E_N = E_g - \frac{R^*}{N^2}, \quad (2)$$

where E_N is the energy of N^{th} excitonic level, $R^* = R_0\mu/m_0\varepsilon_{\text{eff}}^2$, R_0 is the atomic Rydberg, m_0 is the free electron mass and ε_{eff} is the relative dielectric constant. The fit of the inter

Landau level transitions provides an accurate estimation of μ , which in this second step is taken as a fixed parameter. This provides strong limits on the value of R^* , which is further constrained by the observation of the 2s state, well resolved only in high magnetic field both for CsPbI_3 and CsPbBr_3 . Contrary to early magneto optical estimates of exciton binding energies of hybrid organic-inorganic perovskite,^{42,43} our approach does not require us to assume a value for the effective dielectric constant, which we can actually determine from Eq.(2). The values of the effective mass and R^* obtained for all three compounds are summarized in table 1 and Fig 5(a-b).

In the case of organic-inorganic perovskites, the phase transition to a higher symmetry crystalline structure allows the rotational motion of the organic cation, which enhances the dielectric screening and reduces the exciton binding energy.^{32-34,39} The lack of an abrupt change of the band gap observed here implies that inorganic perovskites do not undergo phase transitions up to room temperature. The absence of a structural change suggests that the exciton binding energy does not vary over the investigated temperature interval. To support this conclusion, we have performed magneto-transmission measurements of CsPbBr_3 at 180 K. We compare the magnetic field dependence of the 1s transition energy at high and low temperatures in Fig. 4. The temperature induced change in the band gap has been removed by plotting the high temperature data on a different scale (right axis) but over the same range (10 meV in both cases). The excellent overlap of the two sets of the data demonstrates that the exciton binding energy does not change within experimental accuracy.

In Fig. 5(b) we plot the experimentally determined values of the exciton reduced mass μ of Caesium compounds. Our results are close to theoretical prediction of μ for CsPbI_3 , which range from $\sim 0.07m_0$ ^{44,45} to $\sim 0.18m_0$ ⁴⁶ and in excellent agreement with density functional theory of organic-inorganic perovskites adjusted to fit the experimental band gap.⁴⁷ We compare our results on fully inorganic compounds to the reduced masses determined on organic-inorganic perovskites.^{32,33,39} We observe an increase of the effective mass with

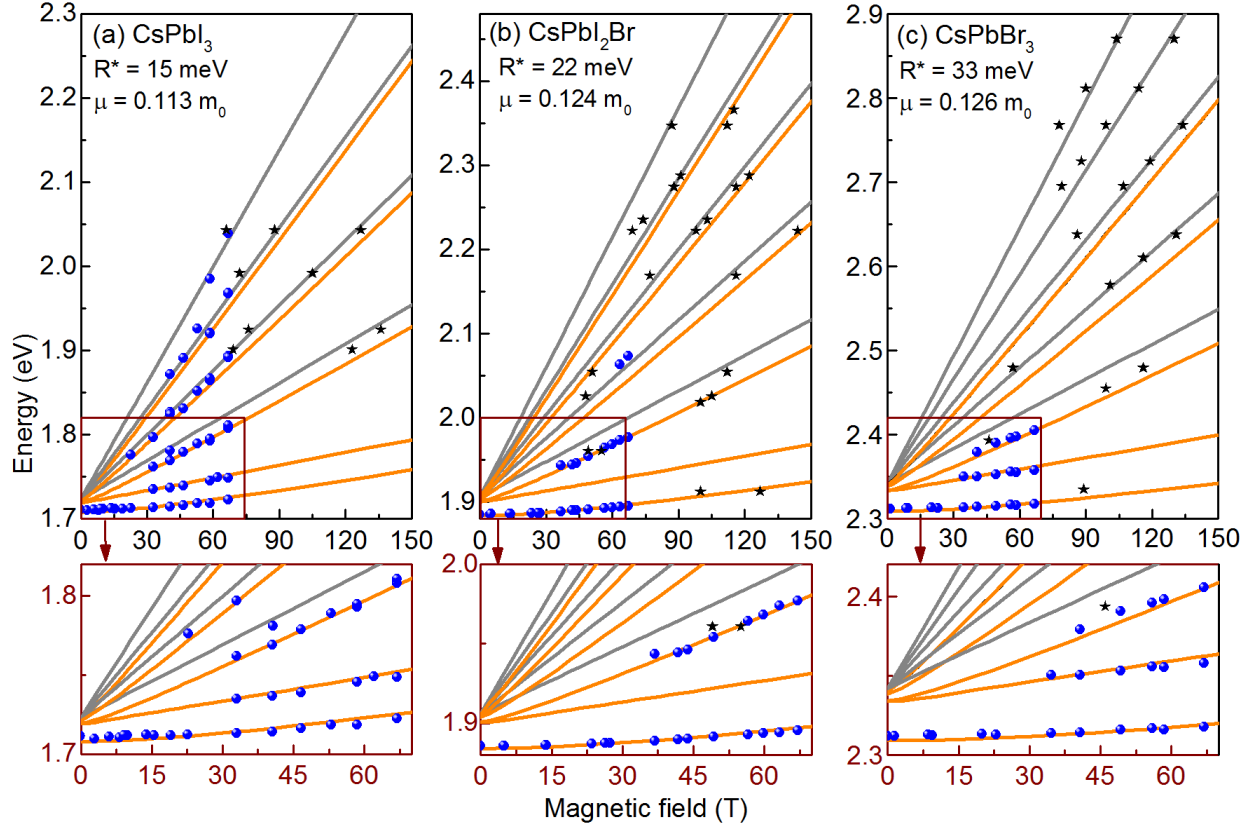


Figure 3: Energy fan chart. Excitonic transition and inter Landau level transition energies as a function of magnetic field at 2 K for (a) CsPbI₃, (b) CsPbI₂Br and (c) CsPbBr₃. Orange lines are the results of the fit to hydrogen-like transitions. Grey lines indicate fitting result of the interband transition between Landau levels. Circles are data from long pulse field measurements and stars are data from single-turn short pulse measurements. The lower panels show an expanded view of the low field and low energy portion of the fan chart.

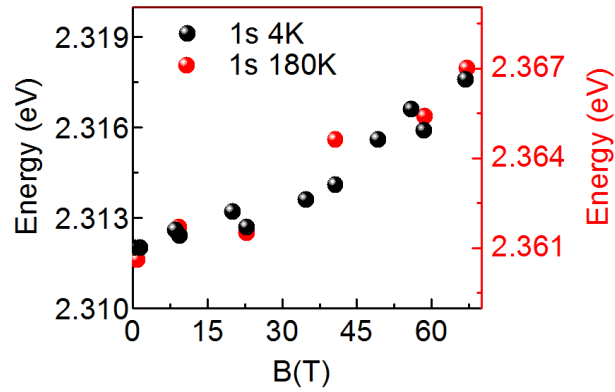


Figure 4: Magnetic field dependence of 1s transition in CsPbBr₃ at two different temperatures.

increasing value of the band gap. This trend can be understood in the frame of a simple two-band $\mathbf{k} \cdot \mathbf{p}$ model,⁴⁸ assuming the same effective mass for the valence and conduction band, the reduced mass of the exciton can be written as

$$\frac{1}{\mu} = \frac{4|P|^2}{m_0 E_g}, \quad (3)$$

where $P = \langle \Psi_{\text{VB}} | p_x | \Psi_{\text{CB}} \rangle$ is the momentum matrix element which couples states in the conduction and valence bands and $2|P|^2/m_0$ is the Kane energy.³³ The measured evolution of the band gap with the reduced mass is well fitted with a Kane energy of 8.3 eV, only slightly larger than theoretical predictions.⁴⁹

Knowing the values of exciton binding energy and the reduced effective mass we can calculate the effective dielectric constant ϵ_{eff} . In Fig. 5(c), we compare the dielectric constant for Caesium-based compounds (stars) with the corresponding quantities for the hybrid organic-inorganic materials from our previous work^{32,33,39} (blue circles). The dielectric constant does not vary significantly for a given lead-halide cage, regardless of the cation, while it decreases with decreasing halide mass. This is consistent with theoretical calculations of the complex dielectric function of MA- and CsPbI₃⁵⁰ and with the computed dielectric functions of MASnX₃⁵¹ and MAPbX₃,⁵² which suggest that the main contributions to the dielectric permittivity are due to Pb-X stretching modes and Pb-X-Pb rocking modes.⁵³ Detailed Raman spectroscopy on the MAPbX₃ series (with X=I, Br, Cl) has demonstrated that both Pb-X stretching and Pb-X-Pb rocking modes harden with decreasing halide mass, with the derived dielectric function exhibiting the same trend as observed in Fig. 5(a).⁵⁴ This confirms the qualitative picture that the dielectric screening properties are mainly determined by the lead-halide cage in the low temperature, when the organic cation motions are frozen.

The exciton binding energies we have determined are significantly smaller than early estimates obtained from magneto optical measurements of the 1s excitonic states.⁴² In the absence of any observed phase transitions (see Fig. 1), we argue that the exciton binding

energy will depend only very weakly on the temperature, as demonstrated by the similar diamagnetic shift of the 1s state at 2 K and 170 K in Fig. 4. This suggests that the photo-created carriers in the compounds investigated exhibit essentially a free-carrier behavior at temperatures corresponding to the normal operating conditions of solar cells.

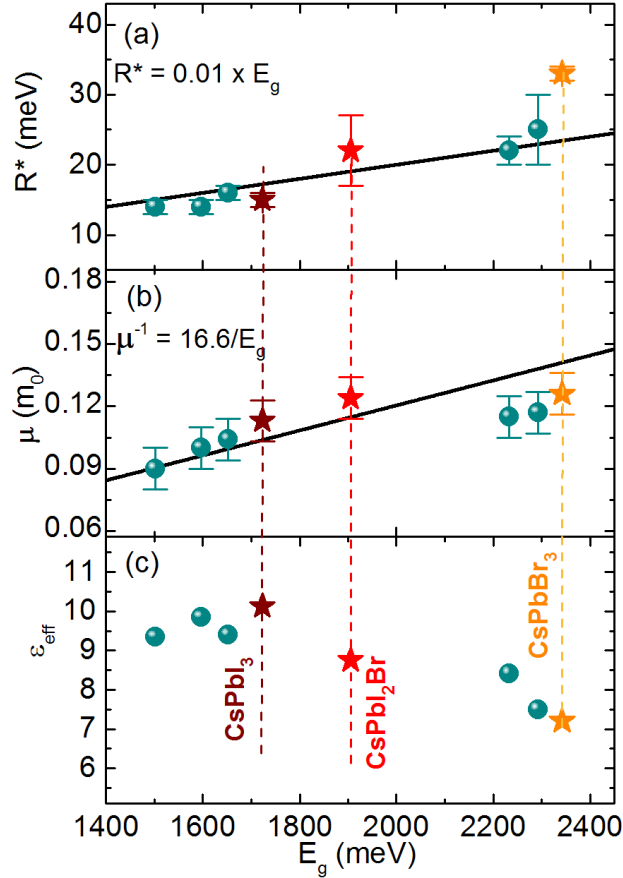


Figure 5: (a) Binding energy, (b) effective mass and (c) dielectric constant as a function of the band gap. Brown, red and yellow stars indicate the results for CsPbI_3 , CsPbI_2Br and CsPbBr_3 , respectively. Blue symbols mark the results from previous work.³³

In summary, we have presented a detailed magneto-optical investigation of fully inorganic CsPbX_3 perovskites ($X=\text{I}$, Br and a mixture of these). The well behaved (continuous) temperature dependence of the band gap points to the absence of any structural phase transitions for perovskites with fully inorganic cations. By performing magneto transmission spectroscopy up to 150 T, we have determined key electronic parameters including the exciton binding energy and reduced mass with high accuracy. Our approach does not require

Table 1: Parameters determined from the fit of the full Landau fan chart for Caesium-based compounds at 2 K.

Compound	Phase	E_g (meV)	R^* (meV)	μ (m_0)	ε_{eff}
CsPbI ₃	cubic	1723	15 ± 1	0.114 ± 0.1	10.0
CsPbI ₂ Br	cubic	1906	22 ± 3	0.124 ± 0.02	8.6
CsPbBr ₃	orthorhombic	2342	33 ± 1	0.126 ± 0.01	7.3

any assumption concerning the strength of the dielectric screening, which we determine a posteriori. The comparison of the values of the dielectric constant for inorganic and hybrid perovskites suggests that the dominant contribution to dielectric screening is related to the relative motion within the lead-halide cage. For the fully inorganic compounds, the values of R^* and μ increase with the band gap energy, similarly to hybrid perovskites. We conclude that at low temperature, when the organic cations are ordered, the qualitative picture of the interactions within the lattice is essentially the same for both the inorganic and hybrid compounds. This is consistent with the ability to optimize perovskite solar cells by adjusting the cation structure while maintaining the same device operation modes.

Experimental Methods

Magneto transmission spectra have been acquired by combining long pulse magnetic field measurements for magnetic fields up to 66 T and short duration pulsed magnets (for magnetic fields up to 150 T). For the long pulse measurements (typical pulse duration ~ 100 ms), the sample was mounted in a liquid helium cryostat. White light from a halogen lamp was used as the excitation source. The light emitted from the lamp was coupled in a 200 μm diameter multimode fiber, used to illuminate the sample. The transmitted light was coupled in a 400 μm diameter multimode fiber and guided to spectrometer equipped with a liquid nitrogen cooled CCD camera. The typical exposure time was 2ms, which ensured that the transmission spectra were acquired at essentially constant magnetic field values. For the very high magnetic field measurements ($B < 150$ T), magnetic field pulses with a typical

duration of 5 μ s were generated by a single turn coil system with a bore diameter of 10 mm. A helium-flow cryostat with a kapton tail was located in the single turn coil. The sample was kept at 5 K. Magneto-transmission measurements were conducted by using a tunable optical parametric oscillator (OPO) pumped by a Ti:sapphire laser as the light source, a fast (100 MHz) silicon detector and a high speed digital oscilloscope.

All samples were prepared on glass microscope slides, which were cleaned by sonication sequentially in acetone and isopropanol, and then treated with oxygen plasma for 10 minutes. The CsPbI₃ and CsPbI₂Br perovskite layers were deposited in a nitrogen glovebox by spincoating (at 1500 rpm) a solution of the appropriate ratios of CsI (Alfa Aesar, 99.9%), PbI₂ (Sigma Aldrich, 99%) and PbBr₂ (Sigma Aldrich, >98%) dissolved at 0.43 M in N,N-Dimethylformamide following a previously reported procedure.³⁵ The CsPbBr₃ perovskite was deposited by sequential evaporation of layers of PbBr₂ (107 nm) and CsBr (93 nm), each deposited at 1-2 $\text{\AA}/\text{s}$ onto room-temperature substrates, at pressures below 6×10^{-6} mbar in a BOC Edwards Auto 306 evaporator. Owing to their limited stability in air at room temperature, CsPbX₃ samples were systematically annealed in an oven before loading them in the cryostat in order to restore the cubic phase. CsPbI₃ was annealed at 350 °C for 10 minutes. CsPbI₂Br and CsPbBr₃ were annealed at 250 °C for 5–7 minutes. After the annealing, the samples were placed in a liquid helium cryostat within 4 minutes, which ensured that the sample remains in the cubic phase. The sample stage was not temperature-controlled. All samples were annealed after deposition and again before measurement.

Acknowledgement

This work was partially supported by ANR JCJC project milliPICS, the Région Midi-Pyrénées under contract MESR 13053031, BLAPHENE and TERASPEC project which received funding from the IDEX Toulouse, Emergence program, NEXT ANR-10-LABX-0037 in the framework of the “Programme des Investissements d’Avenir”. Z. Y. held a fellowship

from the Chinese Scholarship Council (CSC), R. J. S. is a Commonwealth Scholar, funded by the UK government. This work was supported by EPSRC (UK) via its membership to the EMFL (grant no. EP/N01085X/1).

Supporting Information Available

The following files are available free of charge. Supporting information: Low temperature transmission spectra in magnetic field for CsPbI₂Br and CsPbI₃, XRD, Absorbance and PL for CsPbI₃ CsPbI₂Br and CsPbBr₃.

References

- (1) Yang, W. S.; Noh, J. H.; Jeon, N. J.; Kim, Y. C.; Ryu, S.; Seo, J.; Seok, S. I. *Science* **2015**, *348*, 1234–1237.
- (2) Saliba, M.; Matsui, T.; Seo, J.-Y.; Domanski, K.; Correa-Baena, J.-P.; Nazeeruddin, M. K.; Zakeeruddin, S. M.; Tress, W.; Abate, A.; Hagfeldt, A. *Energy & Environmental Science* **2016**, *9*, 1989–1997.
- (3) Saliba, M.; Matsui, T.; Domanski, K.; Seo, J.-Y.; Ummadisingu, A.; Zakeeruddin, S. M.; Correa-Baena, J.-P.; Tress, W. R.; Abate, A.; Hagfeldt, A. *Science* **2016**, *354*, 206–209.
- (4) Shin, S. S.; Yeom, E. J.; Yang, W. S.; Hur, S.; Kim, M. G.; Im, J.; Seo, J.; Noh, J. H.; Seok, S. I. *Science* **2017**, *356*, 167–171.
- (5) Burschka, J.; Pellet, N.; Moon, S.-J.; Humphry-Baker, R.; Gao, P.; Nazeeruddin, M. K.; Grätzel, M. *Nature* **2013**, *499*, 316–319.
- (6) Liu, M.; Johnston, M. B.; Snaith, H. J. *Nature* **2013**, *501*, 395–398.
- (7) Tanaka, K.; Takahashi, T.; Ban, T.; Kondo, T.; Uchida, K.; Miura, N. *Solid state communications* **2003**, *127*, 619–623.

- (8) Deschler, F.; Price, M.; Pathak, S.; Klintberg, L. E.; Jarausch, D.-D.; Higler, R.; Hüttner, S.; Leijtens, T.; Stranks, S. D.; Snaith, H. J.; Atatüre, M.; Phillips, R. T.; Friend, R. H. *The Journal of Physical Chemistry Letters* **2014**, *5*, 1421–1426.
- (9) Huang, H.; Susha, A. S.; Kershaw, S. V.; Hung, T. F.; Rogach, A. L. *Advanced Science* **2015**, *2*, 1500194.
- (10) Stranks, S. D.; Eperon, G. E.; Grancini, G.; Menelaou, C.; Alcocer, M. J.; Leijtens, T.; Herz, L. M.; Petrozza, A.; Snaith, H. J. *Science* **2013**, *342*, 341–344.
- (11) Xing, G.; Mathews, N.; Sun, S.; Lim, S. S.; Lam, Y. M.; Grätzel, M.; Mhaisalkar, S.; Sum, T. C. *Science* **2013**, *342*, 344–347.
- (12) Tan, Z.-K.; Moghaddam, R. S.; Lai, M. L.; Docampo, P.; Higler, R.; Deschler, F.; Price, M.; Sadhanala, A.; Pazos, L. M.; Credgington, D.; Hanusch, F.; Bein, T.; Snaith, H. J.; Friend, R. H. *Nature Nanotechnology* **2014**, *9*, 687–692.
- (13) Zhu, H.; Fu, Y.; Meng, F.; Wu, X.; Gong, Z.; Ding, Q.; Gustafsson, M. V.; Trinh, M. T.; Jin, S.; Zhu, X. *Nature Materials* **2015**, *14*, 636–642.
- (14) Fang, Y.; Dong, Q.; Shao, Y.; Yuan, Y.; Huang, J. *Nature Photonics* **2015**, 679–686.
- (15) Correa-Baena, J.-P.; Abate, A.; Saliba, M.; Tress, W.; Jacobsson, T. J.; Grätzel, M.; Hagfeldt, A. *Energy & Environmental Science* **2017**, *10*, 710–727.
- (16) Roldan-Carmona, C.; Gratia, P.; Zimmermann, I.; Grancini, G.; Gao, P.; Graetzel, M.; Nazeeruddin, M. K. *Energy & Environmental Science* **2015**, *8*, 3550–3556.
- (17) Leijtens, T.; Eperon, G. E.; Noel, N. K.; Habisreutinger, S. N.; Petrozza, A.; Snaith, H. J. *Advanced Energy Materials* **2015**, *5*, 1500963, and other cited there.
- (18) Misra, R. K.; Aharon, S.; Li, B.; Mogilyansky, D.; Visoly-Fisher, I.; Etgar, L.; Katz, E. A. *The Journal of Physical Chemistry Letters* **2015**, *6*, 326–330.

- (19) Hoke, E. T.; Slotcavage, D. J.; Dohner, E. R.; Bowring, A. R.; Karunadasa, H. I.; McGehee, M. D. *Chemical Science* **2015**, *6*, 613–617.
- (20) Koh, T. M.; Fu, K.; Fang, Y.; Chen, S.; Sum, T.; Mathews, N.; Mhaisalkar, S. G.; Boix, P. P.; Baikie, T. *The Journal of Physical Chemistry C* **2013**, *118*, 16458–16462.
- (21) Lee, J.-W.; Seol, D.-J.; Cho, A.-N.; Park, N.-G. *Advanced Materials* **2014**, *26*, 4991–4998.
- (22) Li, Z.; Yang, M.; Park, J.-S.; Wei, S.-H.; Berry, J. J.; Zhu, K. *Chemistry of Materials* **2015**, *28*, 284–292.
- (23) Møller, C. K. *Nature* **1958**, *182*, 1436–1436.
- (24) Da Silva, E. L.; Skelton, J. M.; Parker, S. C.; Walsh, A. *Physical Review B* **2015**, *91*, 144107.
- (25) Kulbak, M.; Gupta, S.; Kedem, N.; Levine, I.; Bendikov, T.; Hodes, G.; Cahen, D. *The Journal of Physical Chemistry Letters* **2015**, *7*, 167–172.
- (26) Eperon, G. E.; Paternò, G. M.; Sutton, R. J.; Zampetti, A.; Haghighirad, A. A.; Cacialli, F.; Snaith, H. J. *Journal of Materials Chemistry A* **2015**, *3*, 19688–19695.
- (27) Kulbak, M.; Cahen, D.; Hodes, G. *The Journal of Physical Chemistry Letters* **2015**, *6*, 2452–2456.
- (28) Beal, R. E.; Slotcavage, D. J.; Leijtens, T.; Bowring, A. R.; Belisle, R. A.; Nguyen, W. H.; Burkhard, G. F.; Hoke, E. T.; McGehee, M. D. *The Journal of Physical Chemistry Letters* **2016**, *7*, 746–751.
- (29) Yi, C.; Luo, J.; Meloni, S.; Boziki, A.; Ashari-Astani, N.; Grätzel, C.; Zakeeruddin, S. M.; Röthlisberger, U.; Grätzel, M. *Energy & Environmental Science* **2016**, *9*, 656–662.

- (30) Lee, J.-W.; Kim, D.-H.; Kim, H.-S.; Seo, S.-W.; Cho, S. M.; Park, N.-G. *Advanced Energy Materials* **2015**, *5*, 1501310.
- (31) McMeekin, D. P.; Sadoughi, G.; Rehman, W.; Eperon, G. E.; Saliba, M.; Horantner, M. T.; Haghighirad, A.; Sakai, N.; Korte, L.; Rech, B.; Johnston, M. B.; Herz, L. M.; Snaith, H. J. *Science* **2016**, *351*, 151–155.
- (32) Miyata, A.; Mitiglu, A.; Plochocka, P.; Portugall, O.; Tse-Wei Wang, J.; Stranks, S. D.; Snaith, H. J.; Nicholas, R. J. *Nature Physics* **2015**, *11*, 582–U94.
- (33) Galkowski, K.; Mitiglu, A.; Miyata, A.; Plochocka, P.; Portugall, O.; Eperon, G. E.; Wang, J. T.-W.; Stergiopoulos, T.; Stranks, S. D.; Snaith, H. J.; Nicholas, R. J. *Energy Environ. Sci.* **2016**, *9*, 962–970.
- (34) Poglitsch, A.; Weber, D. *The Journal of Chemical Physics* **1987**, *87*, 6373–6378.
- (35) Sutton, R. J.; Eperon, G. E.; Miranda, L.; Parrott, E. S.; Kamino, B. A.; Patel, J. B.; Hörantner, M. T.; Johnston, M. B.; Haghighirad, A. A.; Moore, D. T.; Snaith, H. J. *Advanced Energy Materials* **2016**, 1502458.
- (36) Yamada, Y.; Nakamura, T.; Endo, M.; Wakamiya, A.; Kanemitsu, Y. *IEEE Journal of Photovoltaics* **2015**, *5*, 401–405.
- (37) D’Innocenzo, V.; Grancini, G.; Alcocer, M. J.; Kandada, A. R. S.; Stranks, S. D.; Lee, M. M.; Lanzani, G.; Snaith, H. J.; Petrozza, A. *Nature Communications* **2014**, *5*, 3586.
- (38) Galkowski, K.; Mitiglu, A.; Surrente, A.; Yang, Z.; Maude, D.; Kossacki, P.; Eperon, G.; Wang, J.; Snaith, H.; Plochocka, P.; Nicholas, R. *Nanoscale* **2017**, *9*, 3222.
- (39) Yang, Z.; Surrente, A.; Galkowski, K.; Bruyant, N.; Maude, D. K.; Haghighirad, A. A.; Snaith, H. J.; Plochocka, P.; Nicholas, R. J. *J. Phys. Chem. Lett.* **2017**, *8*, 1851–1855.

- (40) Stoumpos, C. C.; Malliakas, C. D.; Peters, J. A.; Liu, Z.; Sebastian, M.; Im, J.; Chasapis, T. C.; Wibowo, A. C.; Chung, D. Y.; Freeman, A. J.; Wessels, B. W.; G, K. M. *Crystal Growth & Design* **2013**, *13*, 2722–2727.
- (41) Makado, P. C.; McGill, N. C. *Journal of Physics C: Solid State Physics* **1986**, *19*, 873.
- (42) Hirasawa, M.; Ishihara, T.; Goto, T.; Uchida, K.; Miura, N. *Physica B: Condensed Matter* **1994**, *201*, 427 – 430.
- (43) Tanaka, K.; Takahashi, T.; Ban, T.; Kondo, T.; Uchida, K.; Miura, N. *Solid State Communications* **2003**, *127*, 619 – 623.
- (44) Chang, Y.; Park, C.; Matsuishi, K. *Journal-Korean Physical Society* **2004**, *44*, 889–893.
- (45) Amat, A.; Mosconi, E.; Ronca, E.; Quarti, C.; Umari, P.; Nazeeruddin, M. K.; Grätzel, M.; De Angelis, F. *Nano Letters* **2014**, *14*, 3608–3616.
- (46) Giorgi, G.; Fujisawa, J.-I.; Segawa, H.; Yamashita, K. *The Journal of Physical Chemistry C* **2014**, *118*, 12176–12183.
- (47) Umari, P.; Mosconi, E.; De Angelis, F. *Scientific Reports* **2014**, *4*, 4467.
- (48) Even, J.; Pedesseau, L.; Katan, C.; Kepenekian, M.; Lauret, J.-S.; Saponi, D.; Delporte, E. *The Journal of Physical Chemistry C* **2015**, *119*, 10161–10177.
- (49) Even, J.; Pedesseau, L.; Katan, C. *The Journal of Physical Chemistry C* **2014**, *118*, 11566–11572.
- (50) Berdiyorov, G. R.; Kachmar, A.; El-Mellouhi, F.; Carignano, M. A.; El-Amine Madjet, M. *The Journal of Physical Chemistry C* **2016**, *120*, 16259–16270.
- (51) Feng, J.; Xiao, B. *The Journal of Physical Chemistry C* **2014**, *118*, 19655–19660.
- (52) Feng, J.; Xiao, B. *The journal of physical chemistry letters* **2014**, *5*, 1278–1282.

- (53) Pérez-Osorio, M. A.; Milot, R. L.; Filip, M. R.; Patel, J. B.; Herz, L. M.; Johnston, M. B.; Giustino, F. *J. Phys. Chem. C* **2015**, *119*, 25703–25718.
- (54) Sendner, M.; Nayak, P. K.; Egger, D. A.; Beck, S.; Müller, C.; Epding, B.; Kowalsky, W.; Kronik, L.; Snaith, H. J.; Pucci, A.; Lovrincic, R. *Materials Horizons* **2016**, *3*, 613–620.

Graphical TOC Entry

